



HAL
open science

Heart failure-induced cognitive dysfunction is mediated by intracellular Ca²⁺ leak through ryanodine receptor type 2

Haikel Dridi, Yang Liu, Steven Reiken, Xiaoping Liu, Elentina Argyrousi, Qi Yuan, Marco Miotto, Leah Sittenfeld, Andrei Meddar, Rajesh Kumar Soni, et al.

► **To cite this version:**

Haikel Dridi, Yang Liu, Steven Reiken, Xiaoping Liu, Elentina Argyrousi, et al.. Heart failure-induced cognitive dysfunction is mediated by intracellular Ca²⁺ leak through ryanodine receptor type 2. Nature Neuroscience, In press, 10.1038/s41593-023-01377-6 . hal-04158307

HAL Id: hal-04158307

<https://hal.science/hal-04158307v1>

Submitted on 11 Jul 2023

HAL is a multi-disciplinary open access archive for the deposit and dissemination of scientific research documents, whether they are published or not. The documents may come from teaching and research institutions in France or abroad, or from public or private research centers.

L'archive ouverte pluridisciplinaire **HAL**, est destinée au dépôt et à la diffusion de documents scientifiques de niveau recherche, publiés ou non, émanant des établissements d'enseignement et de recherche français ou étrangers, des laboratoires publics ou privés.

Heart failure-induced cognitive dysfunction is mediated by intracellular Ca²⁺ leak through ryanodine receptor type 2

Haikel Dridi 1 , Yang Liu 1, Steven Reiken 1, Xiaoping Liu¹, Elentina K. Argyrousi 2, Qi Yuan¹, Marco C. Miotto 1, Leah Sittenfeld , Andrei Meddar , Rajesh Kumar Soni³, Ottavio Arancio ^{2,4,5}, Alain Lacampagne^{6,7} & Andrew R. Marks 1

1 Department of Physiology and Cellular Biophysics, Clyde and Helen Wu Center for Molecular Cardiology, Columbia University Vagelos College of Physicians & Surgeons, New York, NY, USA.

2 Taub Institute for Research on Alzheimer's Disease and the Aging Brain, Columbia University, New York, NY, USA.

3 Proteomics and Macromolecular Crystallography Shared Resource, Herbert Irving Comprehensive Cancer Center, New York, NY, USA.

4 Department of Medicine, Columbia University, New York, NY, USA.

5 Department of Pathology and Cell Biology, Columbia University, New York, NY, USA.

6 PHYMEDEXP, University of Montpellier, CNRS, INSERM, CHU Montpellier, Montpellier, France.

7 LIA1185 CNRS, Montpellier, France.

e-mail: dh2756@cumc.columbia.edu; arm42@cumc.columbia.edu

Cognitive dysfunction (CD) in heart failure (HF) adversely affects treatment compliance and quality of life. Although ryanodine receptor type 2 (RyR2) has been linked to cardiac muscle dysfunction, its role in CD in HF remains unclear. Here, we show in hippocampal neurons from individuals and mice with HF that the RyR2/intracellular Ca²⁺ release channels were subjected to post-translational modification (PTM) and were leaky. RyR2 PTM included protein kinase A phosphorylation, oxidation, nitrosylation and depletion of the stabilizing subunit calstabin2. RyR2 PTM was caused by hyper-adrenergic signaling and activation of the transforming growth factor-beta pathway. HF mice treated with a RyR2 stabilizer drug (S107), beta blocker (propranolol) or transforming growth factor-beta inhibitor (SD-208), or genetically engineered mice resistant to RyR2 Ca²⁺ leak (RyR2-p.Ser2808Ala), were protected against HF-induced CD. Taken together, we propose that HF is a systemic illness driven by intracellular Ca²⁺ leak that includes cardiogenic dementia.

HF is the most rapidly growing cardiovascular disorder affecting millions worldwide^{1,2}, with associated high rates of mortality, poor quality of life, and high health care costs due to decreased cardiac function and dysfunction of other organ systems^{3–5}. Recent studies suggest that CD in HF, known as ‘cardiogenic dementia’ may be caused by HF itself, with a prevalence of 20–80%^{6,7}.

CD includes forgetfulness and poor learning ability, which may impair self-care^{8–10} and compliance^{11,12} in as many as 90% of those with HF. Noncompliance increases the risk of mortality and morbidity¹³. Indeed, CD impairs the ability of individuals with HF to make decisions in critical situations, such as early recognition and interpretation of worsening symptoms, and making appropriate decisions about their health. People with HF and preserved ejection fraction also exhibit CD¹⁴, including verbal memory and executive function deficits, known as cognitive inflexibility¹⁵. Structural changes in the brain including atrophy, increased white matter hyper-intensities, gray matter loss and silent cerebral infarction, are frequently observed in HF patients with CD^{16,17}. Interestingly, these structural and functional changes coincide with a chronic inflammatory response and neurohormonal activation including the renin–angiotensin–aldosterone system and the adrenergic pathway¹⁸. Furthermore, clinical studies have linked cardiovascular diseases, dementia and Alzheimer’s disease through common triggers, including inflammation, oxidative stress, hypoxia¹⁹ and adrenergic signaling^{20–22}.

Indeed, norepinephrine modulates the levels of consciousness^{23,24}. The sympathetic nervous system is continuously activated in patients with HF²⁵ and is known to be part of a major upstream signaling pathway that alters intracellular Ca²⁺ homeostasis and tightly controls neuronal cellular function and survival. Ca²⁺ dyshomeostasis is a hallmark of neurodegenerative diseases, including Alzheimer’s disease²⁶, Huntington’s disease²⁷ and Parkinson’s disease²⁸. Intracellular Ca²⁺ signaling plays a role in regulating long-term potentiation (LTP), long-term depression and neurodegeneration^{29–31}.

In neurons, activation of inositol-1,4,5-trisphosphate receptors (IP3Rs) and RyRs amplifies intracellular Ca²⁺ signals³². Increased intracellular Ca²⁺ concentration activates Ca²⁺-dependent processes involved in plasticity and synaptic transmission that are required for learning and memory³³. RyR2, the Ca²⁺-activated intracellular Ca²⁺ release channel on the sarcoplasmic reticulum (SR) or endoplasmic reticulum (ER), is a homotetrameric macromolecular protein complex that includes four RyR2 monomers, 565-kDa polypeptide each³⁴. The RyR2 channel is regulated by kinases and phosphatases³⁵, phosphodiesterase³⁶, calmodulin³⁷, and the stabilizing subunit calstabin2 (FKBP12.6)³⁵. Protein kinase A (PKA) and Ca²⁺/calmodulin-dependent protein kinase II (CAMKII) tether to RyR2 and phosphorylate the channel at Ser2808 and Ser2814, respectively^{35,38}. PKA hyperphosphorylation and/or oxidation/nitrosylation of RyR2 cause calstabin2 dissociation, leading to leaky channels that do not close properly^{35,39}.

We⁴⁰ and others have previously reported that RyR channels are dysfunctional not only in the cardiomyocytes of patients with HF^{35,41} but also in the skeletal muscle^{42,43}, suggesting the existence of a common mechanism that primarily affects RyR2 in the cardiac muscle and propagates to affect RyRs in other organs expressing different isoforms of the channels, such as RyR2 in the pancreatic beta cells⁴⁴ (may cause diabetes) and in the brain (may impair cognitive function), and RyR1 in the diaphragm/lung (may cause respiratory disorders) and locomotor muscle (may cause exercise intolerance and muscle fatigue).

In this study, we found that the hyper-adrenergic state and the enhanced inflammatory response in HF caused neuronal RyR2-mediated intracellular Ca²⁺ leak that subsequently affected cognition and memory. Neuronal Ca²⁺ dyshomeostasis increased mitochondrial Ca²⁺ content, contributing to oxidative overload, and altered the expression of key genes involved in cognitive function. Stabilizing leaky RyR2 channels using a small-molecule Rycal drug S107 prevented cognitive impairment induced by HF.

Results

Neuronal RyR2 channels are leaky in individuals with heart failure

To evaluate RyR2 in the brains of individuals with HF, hippocampal biopsy samples from controls (non-HF) and de-identified individuals with HF (Supplementary Tables 1 and 2) were obtained from the Brain Bank at Columbia University and the National Institutes of Health (NIH) Neuro-Biobank. Immunoprecipitated RyR2 and isolated ER fractions were used to analyze the composition of the hippocampal RyR2 macromolecular complex and PTMs known to be associated with RyR channel Ca²⁺ leak^{31,32,35}. Hippocampal RyR2 from individuals with HF ($n = 9$) exhibited PKA hyper-phosphorylation (on Ser2808), oxidation, cysteine nitrosylation, and were depleted of calstabin2, compared to controls ($n = 4$; Fig. 1a,b). This is the ‘biochemical signature’ of ‘leaky’ RyR2 channels^{35,45}. Single-channel recordings of hippocampal RyR2, reconstituted into planar lipid bilayers, revealed increased open probability (P_o), increased mean open time (T_o) and decreased mean closed time (T_c) in individuals with HF compared to controls ($P_o = 0.19\% \pm 0.02\%$, $T_o = 18 \pm 2$ ms, $T_c = 58 \pm 5$ ms in HF hippocampi, $n = 9$; versus $P_o = 0.01\% \pm 0.002\%$, $T_o = 2 \pm 0.2$ ms, $T_c = 515 \pm 52$ ms in controls, $n = 4$; $P < 0.05$) in the presence of low, non-activating [Ca²⁺]_{cis} (150 nM), conditions under which normal RyR2 channels are tightly closed (Fig. 1c,d). This elevated P_o is consistent with pathological hippocampal ER Ca²⁺ leak^{26,31}. Indeed, neuronal microsomes from individuals with HF exhibited increased RyR-mediated ER Ca²⁺ leak compared with controls (Fig. 1e,f).

Impaired cognitive function in mouse model of heart failure

Because of the complexity of the clinical manifestation of HF patients, we used the mouse model of HF (myocardial infarction, MI) with reduced ejection fraction⁴⁶ (Supplementary Table 3) to evaluate the mechanisms of CD. We used the open field test and elevated plus maze (EPM) test to evaluate the behavioral phenotypes, and spontaneous exploratory activity in the mice^{31,47}. In the open field test, mice were placed at the center of a chamber and allowed to explore for 6 min. Within the first and the second 3 min, the ratio of time spent in the center versus periphery area for MI mice was similar (0.22 ± 0.02 and 0.28 ± 0.03 , $n = 22$, $P = 0.18$), whereas these ratios were significantly different in the SHAM group (0.1 ± 0.01 and 0.28 ± 0.04 , $n = 13$, $P < 0.05$; Fig. 2a). In the EPM test, MI mice spent more time in the open arms of the EPM (Fig. 2b) compared to SHAM (0.22 ± 0.04 versus 0.14 ± 0.02 ; $P < 0.05$). The abnormal behaviors were prevented by the pharmacological treatments using the RyR2 stabilizer Rycal compound S107, the nonselective beta-adrenergic antagonist propranolol, and the anti-inflammatory transforming growth factor-beta (TGF- β) inhibitor SD-208 (Fig. 2a,b). As a control, we tested the effects of a closely related Rycal ARM036, which has the same mechanism of action as S107 but does not cross the blood–brain barrier (BBB)²⁷. ARM036 had no effect on MI mouse cognitive performance in either task (Fig. 2a,b) indicating that the S107 effects were at the CNS level rather than the systemic level.

Next, a novel object recognition test was used to evaluate hippocampal-dependent short-term memory^{31,48}. MI mice showed significantly lower discrimination index (15% \pm 4%) compared to the SHAM group (48% \pm 5%, $P < 0.05$; Fig. 2c). S107, propranolol and SD-208 treatments prevented short-term memory loss by increasing the discrimination index to 46% \pm 4%, 46% \pm 6% and 35% \pm 6%, respectively ($P < 0.05$), whereas ARM036 did not increase the discrimination index (15% \pm 3%; $P = 0.25$; Fig. 2c).

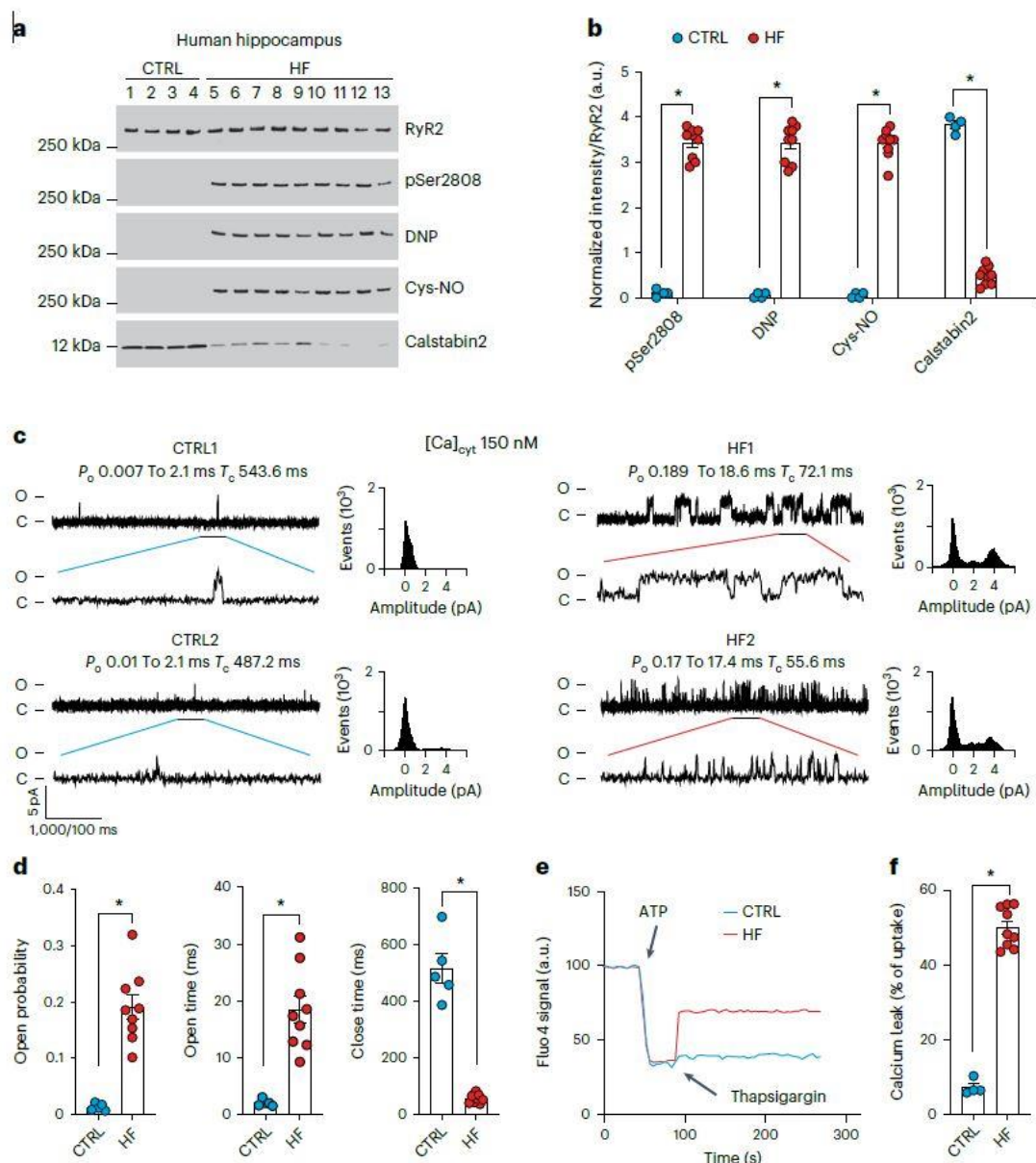


Fig. 1 | Hippocampal RyR2 channels are remodeled and leaky in patients with heart failure. **a,b**, Representative SDS-PAGE analysis and quantification of modified RyR2 and calstabin2 immunoprecipitated from hippocampi of controls and individuals with HF (IP RyR2; bands normalized to total RyR2). Control (CTRL), $n = 4$; HF, $n = 9$. **c**, Single-channel recordings of RyR2 incorporated in planar lipid bilayers with 150 nM Ca^{2+} in the *cis* chamber, corresponding to representative experiments performed using human hippocampal samples from controls and HF patients (two traces from two different controls and individuals with HF are shown) **d**, P_o , T_o and T_c of RyR2 channels in controls ($n = 5$) and HF ($n = 9$) hippocampi. **e**, ER Ca^{2+} leak measured in microsomes from control ($n = 4$) and HF participant ($n = 9$) hippocampi. **f**, Bar graphs represent the quantification of microosomal Ca^{2+} leak as the percentage of uptake in controls ($n = 5$) and HF individuals ($n = 9$). Individual values are shown with the mean \pm s.e.m. (t -test $*P < 0.05$, controls versus HF individuals). Data are derived from biologically independent samples. All statistical tests were two sided. a.u., arbitrary units.

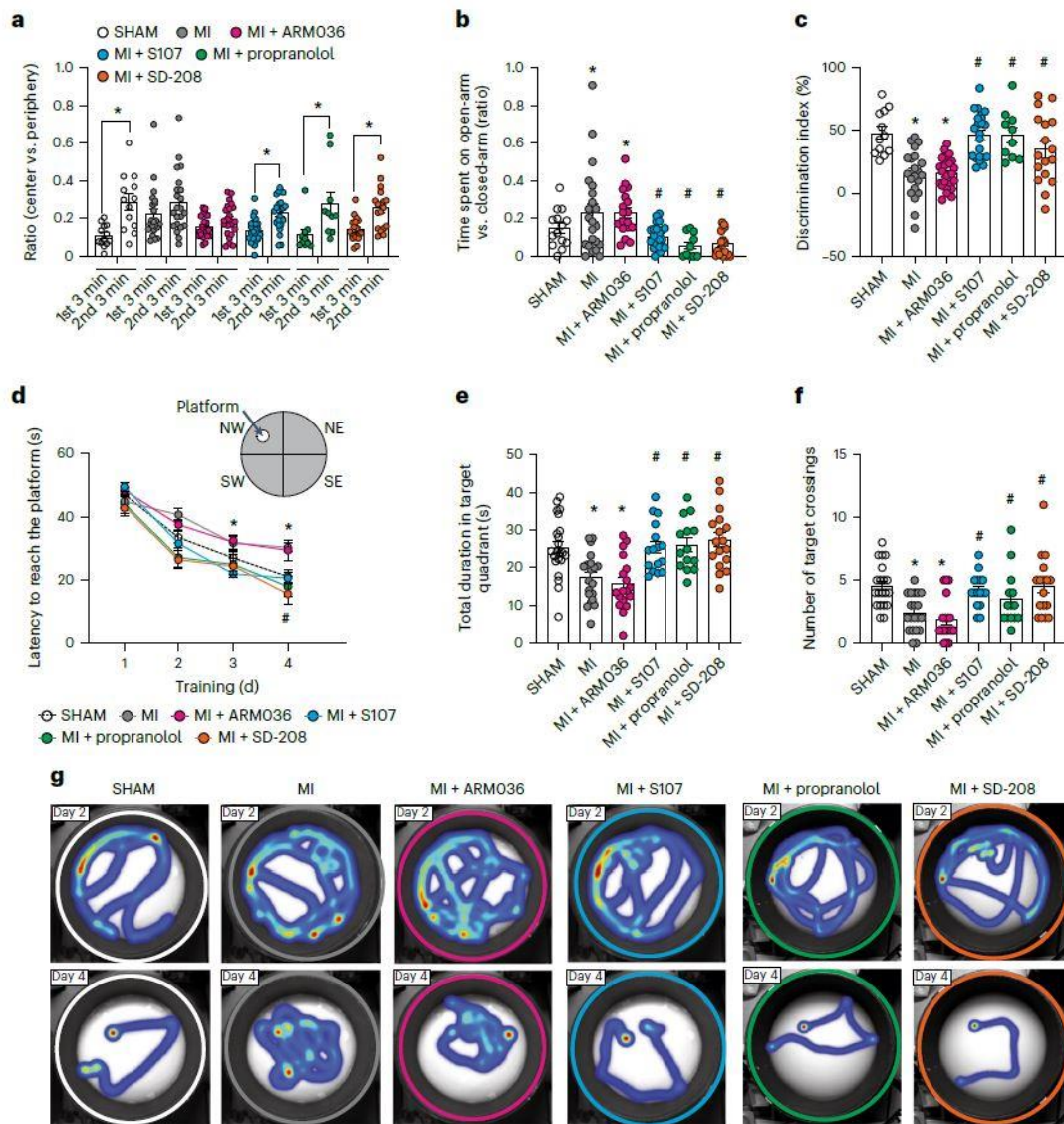


Fig. 2 | Mouse model of heart failure (myocardial infarction) is associated with cognitive dysfunction. **a**, Open field test of mice operated SHAM ($n = 13$), MI ($n = 22$), MI treated with ARM036 (MI + ARM036, $n = 23$), MI treated with S107 (MI + S107, $n = 24$), MI treated with propranolol (MI + propranolol, $n = 10$) and MI treated with TGF- β inhibitor (MI + SD-208, $n = 18$). Ratios of total time spent in the center area versus periphery area within first 3 min and second 3 min are shown. **b**, EPM test showing the ratios of time spent in the open-arm versus closed-arm in SHAM ($n = 14$), MI ($n = 22$), MI + ARM036 ($n = 18$), MI + S107 ($n = 23$), MI + propranolol ($n = 10$) and MI + SD-208 ($n = 18$) mice. **c**, Novel object recognition test showing the discrimination index in SHAM ($n = 12$), MI ($n = 21$), MI + ARM036 ($n = 23$), MI + S107 ($n = 22$), MI + propranolol ($n = 10$) and MI + SD-208 ($n = 17$) mice. **d**, MWM test (learning curves for 4 d) in SHAM ($n = 22$), MI ($n = 20$), MI + ARM036 ($n = 19$), MI + S107 ($n = 19$), MI + propranolol ($n = 14$) and MI + SD-208 ($n = 19$) mice. **e**, Probe trials after escape platform removed showing the total duration spent in the target quadrant at day 5 in SHAM ($n = 22$), MI ($n = 20$), MI + ARM036 ($n = 18$), MI + S107 ($n = 17$), MI + propranolol ($n = 14$) and MI + SD-208 ($n = 17$) mice. **f**, Number of target crossings at day 5 in SHAM ($n = 20$), MI ($n = 20$), MI + ARM036 ($n = 18$), MI + S107 ($n = 16$), MI + propranolol ($n = 14$) and MI + SD-208 ($n = 17$) mice. **g**, Heat maps showing the latency for each group at day 2 and day 4. Individual values are shown with mean \bullet } s.e.m. Two-tailed t -test $*P < 0.05$ in **a** shows significance between the first 3 min and second 3 min of each group. One-way analysis of variance (ANOVA) was used to compare the difference between the six groups in **b**, **c**, **e** and **f**; Tukey's test was used for multiple comparisons; two-way ANOVA was used in **d**. Tukey's test post hoc correction for multiple comparisons was used. $*P < 0.05$, SHAM versus MI or MI + ARM036; $\#P < 0.05$, MI versus MI + S107, MI + propranolol or MI + SD-208. All statistical tests were two sided. Data are derived from biologically independent samples.

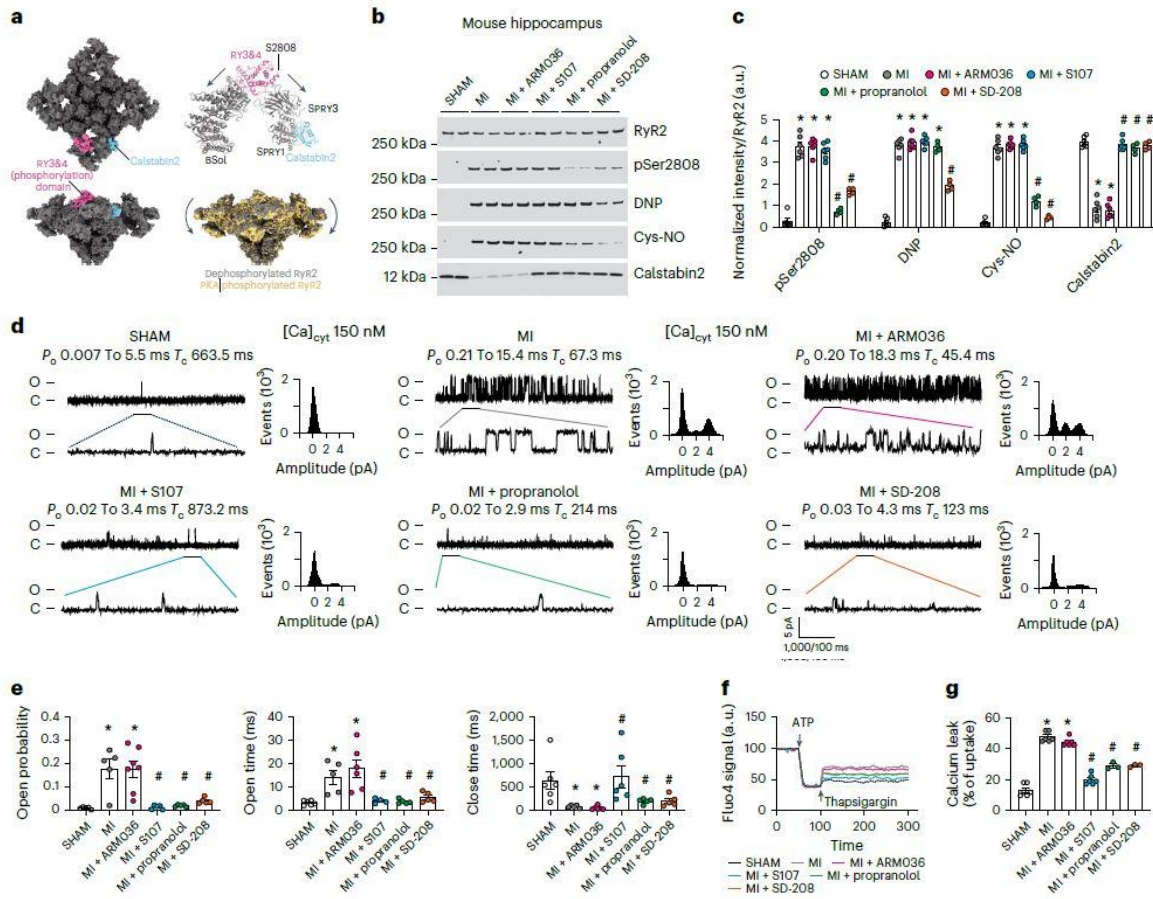


Fig. 3 | Mouse model of heart failure is associated with leaky hippocampal RyR2. **a**, Cryogenic electron microscopy structure of RyR2 (gray, top and side view) showing the location of the Ser2808 in the RY3&4 phosphorylation domain (magenta) and calstabin2 (cyan). RyR2 PKA phosphorylation shifted the channel toward a primed state (yellow)50. **b,c**, Representative SDS-PAGE analysis and quantification of modified RyR2 and calstabin2 immunoprecipitated from hippocampal RyR2 complex (IP RyR2; bands normalized to total RyR2) in SHAM ($n = 6$), MI ($n = 6$), MI + ARM036 ($n = 6$), MI + S107 ($n = 6$), MI + propranolol ($n = 4$) and MI + SD-208 ($n = 4$) mice. **d**, Single-channel traces of RyR2 incorporated in planar lipid bilayers with 150 nM Ca²⁺ in the *cis* chamber, corresponding to representative experiments performed with hippocampal samples from SHAM ($n = 6$), MI ($n = 5$), MI + ARM036 ($n = 6$), MI + S107 ($n = 5$), MI + propranolol ($n = 5$) and MI + SD-208 ($n = 5$) mice. **e**, RyR2 P_o , T_o and T_c in the same groups. **f**, Ca²⁺ leak measured in microsomes from mouse hippocampi of the same groups. **g**, Bar graphs represent the quantification of Ca²⁺ leak as the percentage of uptake in SHAM ($n = 6$), MI ($n = 6$), MI + ARM036 ($n = 6$), MI + S107 ($n = 6$), MI + propranolol ($n = 3$) and MI + SD-208 ($n = 3$) mice. Individual values are shown with the mean \pm s.e.m. One-way ANOVA and Tukey's test post hoc correction for multiple comparisons shows * $P < 0.05$, SHAM versus MI or MI + ARM036; # $P < 0.05$, MI versus MI + S107, MI + propranolol or MI + SD-208. Data are derived from biologically independent samples. All statistical tests were two sided.

A Morris water maze (MWM) test was performed to assess hippocampal-dependent long-term spatial learning and memory31,49. MI mice exhibited significantly prolonged latency to find and reach the hidden platform on day 4 training trials (30 \bullet \pm 1 s, $n = 20$) compared to the SHAM controls (21 \bullet \pm 2 s, $P < 0.05$, $n = 22$). S107, propranolol and SD-208 treatments significantly reduced latency on day 4 (20 \bullet \pm 2 s, 17 \bullet \pm 3 s and 15 \bullet } 3 s, respectively, $P < 0.05$, $n = 19$, 14 and 19 per group). Again, MI mice treated with ARM036 did not show significant reduction on the latency to reach the hidden platform (29 \bullet \pm 3 s, $P = 0.99$, $n = 19$; Fig. 2d).

A probe trial was performed on day 5 of the MWM test. MI mice spent a significantly shorter duration in target quadrant (17 ± 1 s, $n = 19$) and exhibited a reduced number of target crossings (2.4 ± 0.3 , $n = 19$) within the 60-s probe trial compared to SHAM (25 ± 2 s and 4.6 ± 0.3 , $P < 0.05$, $n = 20$; Fig. 2e,f). S107, propranolol and SD-208 treatments, but not ARM036, were able to correct the spatial memory deficit in MI by improving the time spent in the target quadrant (26 ± 2 s, 26 ± 2 s and 27 ± 2 s, respectively, $P < 0.05$) and target crossings (4.2 ± 0.3 , 3.5 ± 0.6 and 4.5 ± 0.6 , respectively, $P < 0.05$, $n = 14$ – 19 per group) in the probe trial (Fig. 2e,f). A heat map of the swimming behavior of these mice is shown at days 2 and 4 (Fig. 2g). Of note, the traveled distance and velocity of mice in the open field, EPM and MWM tests were comparable between all the groups (Supplementary Table 4).

Neuronal RyR2 channels are leaky in the mouse model of heart failure

We have recently solved the high-resolution three-dimensional (3D) structure of human RyR2 and showed that the PKA-phosphorylated channels on Ser2808 adopt a primed state (halfway between the closed and the open states), allowing the opening of channels at a lower cytosolic Ca^{2+} concentration resulting in leaky channels⁵⁰ (Fig. 3a). Furthermore, we identified the binding site of the Rycal drugs (S107 and ARM210)^{50,51} on RyR1 and RyR2 and have shown that these drugs are able to reverse the primed state of leaky channels toward a fully closed state⁵⁰. We then evaluated the PTMs and functional abnormalities of neuronal RyR2 in HF hippocampal samples from MI mice and compared them to SHAM. Hippocampal RyR2 was immunoprecipitated and immunoblotted to detect PTMs. Neuronal RyR2 from MI mice exhibited PKA hyper-phosphorylation (on Ser2808, the main PKA-phosphorylation site⁵⁰), oxidation, cysteine nitrosylation and calstabin2 depletion compared to the SHAM hippocampal samples ($P < 0.05$; Fig. 3b,c). Single-channel recordings of neuronal RyR2 from MI mice revealed increased open probability ($P_o = 0.17\% \pm 0.04\%$) in the presence of low non-activating $[\text{Ca}^{2+}]_{\text{cis}}$ (SHAM, $P_o = 0.07\% \pm 0.002\%$, $P < 0.05$). Hippocampal RyR2 from the MI mice also exhibited increased open time and decreased close time (Fig. 3d,e). This elevated P_o is consistent with pathological ER Ca^{2+} leak^{26,31}. Indeed, neuronal microsomes from MI mice exhibited increased RyR-mediated ER Ca^{2+} leak compared with SHAM-operated mice (Fig. 3f,g). Interestingly, PTMs and functional RyR2 remodeling (leak) were comparable to the RyR2 abnormalities observed in human HF hippocampal samples (Fig. 1). S107 treatment (but not ARM036 treatment) restored calstabin2 binding to RyR2 and decreased the hippocampal RyR2 open probability ($P_o = 0.01\% \pm 0.003\%$, $P < 0.05$) and mean open time, and increased mean closed time, and reduced ER Ca^{2+} leak (Fig. 3e–g) indicating that the ability of S107 to cross the BBB was essential to fix the leaky hippocampal RyR2 channels. Propranolol treatment significantly reduced RyR2 phosphorylation, nitrosylation and restored calstabin2 binding to the channels. Meanwhile SD-208 treatment significantly decreased RyR2 phosphorylation, oxidation/nitrosylation and enabled rebinding of calstabin2 to the channels (Fig. 3b,c). Both propranolol and SD-208 treatment decreased RyR2 open probability ($P_o = 0.018\% \pm 0.020\%$ and $0.030\% \pm 0.005\%$ respectively) and mean open time, and increased mean closed time and reduced the ER Ca^{2+} leak compared to the untreated MI mice (Fig. 3e–g). As mentioned above, S107 is a specific RyR2-targeted drug that stabilizes the closed conformation of the channels without effects on PTMs, whereas propranolol and SD-208 prevent RyR2 Ca^{2+} leak by reducing the channel oxidation, nitrosylation and hyper-phosphorylation. Thus, a reduction of RyR2 PTMs and/or stabilization of specific interacting domains of the channels allow calstabin2 to rebind and rescue aberrant RyR2 opening and pathological ER Ca^{2+} leak.

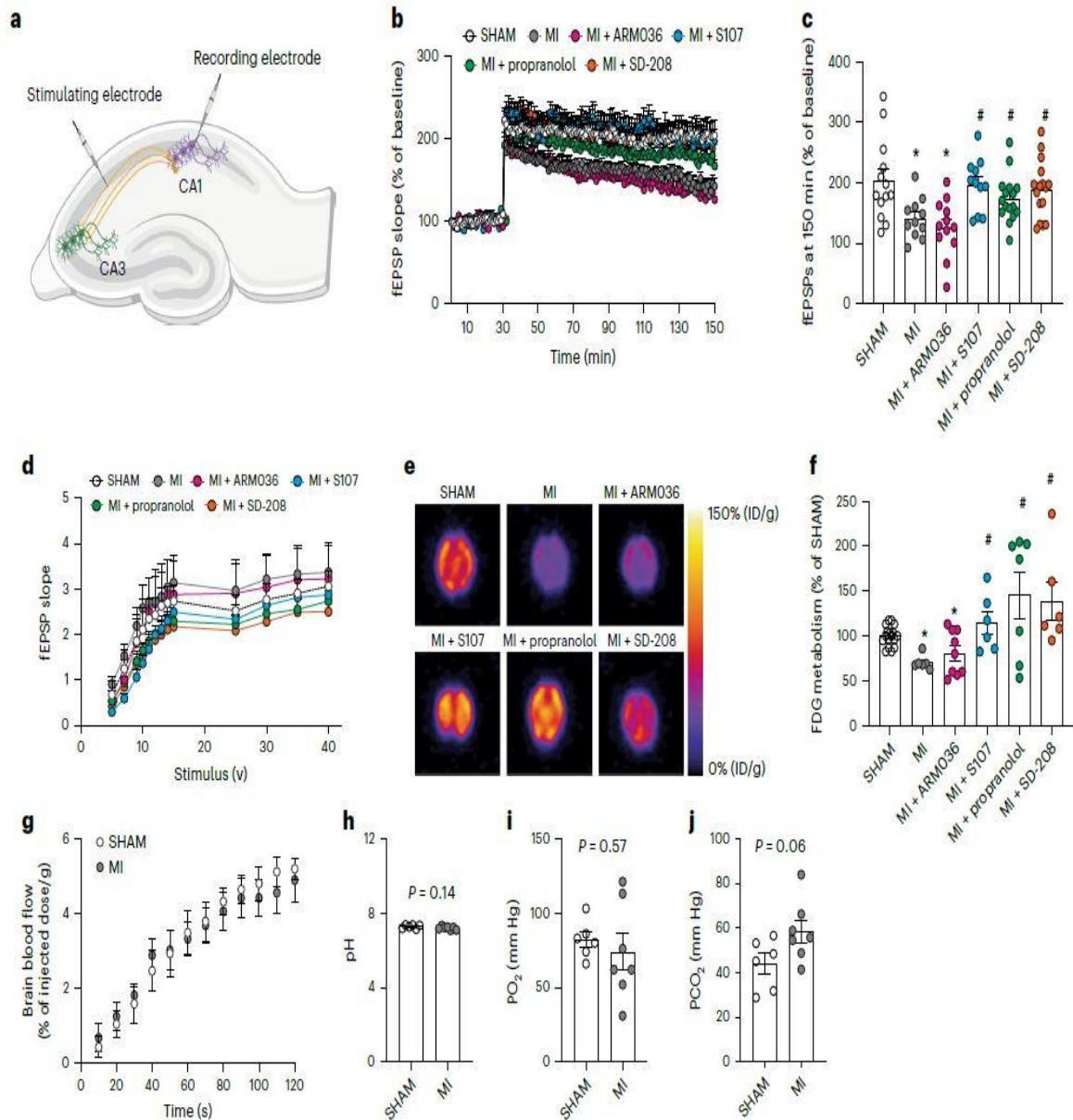


Fig. 4 | Mouse model of heart failure exhibits impaired long-term potentiation and diminished hippocampal glucose uptake. **a**, Schematic representation of a hippocampal brain slice for LTP experiments and the positioning of the stimulating and recording electrodes. **b**, fEPSPs in hippocampal slices from each experimental group (SHAM ($n = 13$), MI ($n = 12$), MI + ARM036 ($n = 12$), MI + S107 ($n = 11$), MI + propranolol ($n = 17$) and MI + SD-208 ($n = 16$)). **c**, fEPSPs at 150 min in all the experimental groups. **d**, Basal neurotransmission (fEPSP slope), which remained unaltered between the different groups. **e**, Representative microPET images of FDG uptake (percentage of injected dose per gram (%ID/g)) in the mouse brains of different groups. **f**, Quantification of FDG uptake in the brains of mice from different experimental groups shown as a percentage of the FDG uptake in the SHAM mice (SHAM ($n = 17$), MI ($n = 6$), MI + ARM036 ($n = 9$), MI + S107 ($n = 6$), MI + propranolol ($n = 7$) and MI + SD-208 ($n = 6$)). **g**, Quantification of 2-min dynamic microPET scans of MI ($n = 4$) and SHAM ($n = 4$) mice demonstrating similar brain blood flow FDG uptake in the brains of both groups of mice during the first 2 min after intravenous injection (%ID/g). **h–j**, pH, PO₂ and PCO₂ blood levels in SHAM ($n = 6$) and MI ($n = 7$) mice. Individual values are shown with the mean \pm s.e.m. One-way ANOVA and Tukey's test post hoc correction for multiple comparisons, * $P < 0.05$, SHAM versus MI or MI + ARM036; # $P < 0.05$, MI versus MI + S107, MI + propranolol or MI + SD-208. A t -test was used in **h–j**. Data are derived from biologically independent samples. All statistical tests were two sided.

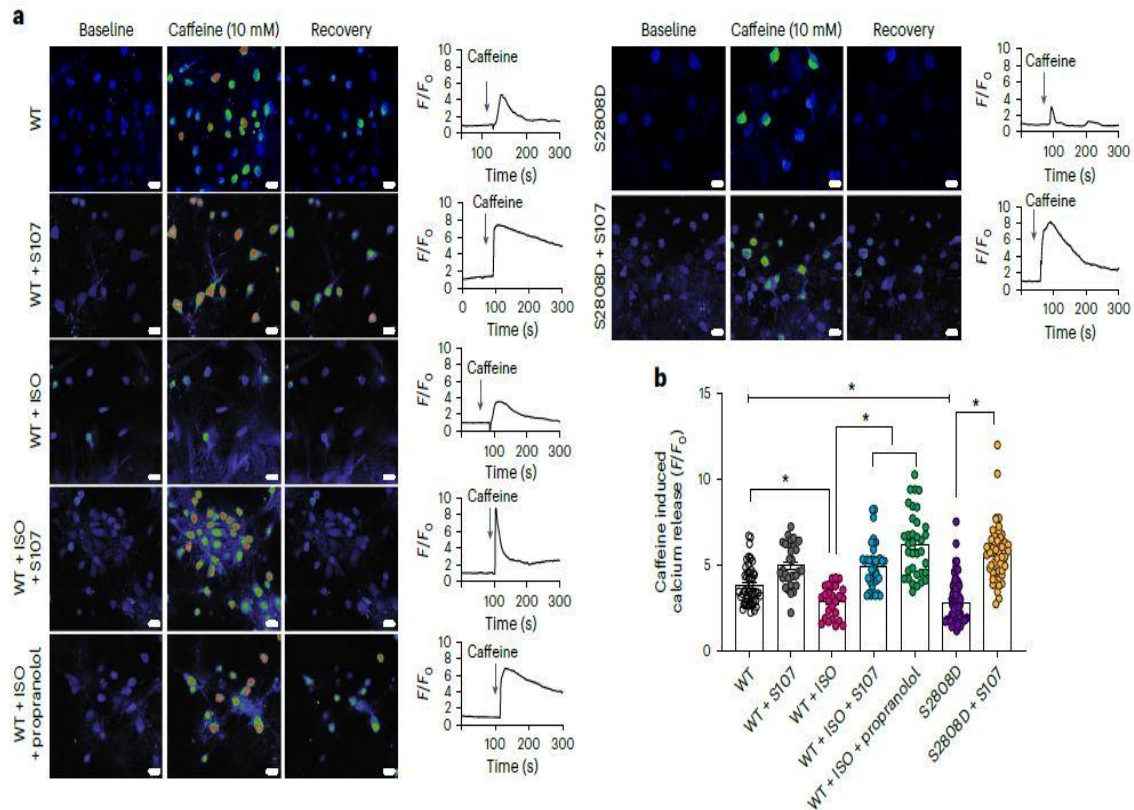


Fig. 5 | Adrenergic agonist and RyR2 Ser2808 phospho-mimetic mutation deplete endoplasmic reticulum Ca^{2+} stores in primary hippocampal neurons. **a**, Representative images of 14-d cultured hippocampal neurons stimulated with 10 mM caffeine. For each condition, the Ca^{2+} levels are shown at baseline, during stimulation and at recovery. **b**, Quantification of caffeine-induced Ca^{2+} release (F/F_0) in response to 10 mM caffeine in neurons from wild-type (WT; $n = 50$), WT + S107 ($n = 30$), WT + isoproterenol (ISO; $n = 26$), WT + ISO + propranolol ($n = 35$), neurons expressing RyR2-p.Ser2808Asp untreated (S2808D; $n = 70$) and treated with S107 (p.Ser2808Asp + S107; $n = 54$). Individual values are shown with the mean \bullet } s.e.m. (t -test $*P < 0.05$). Scale bar, 10 μm . A reduction in caffeine-induced Ca^{2+} release indicates a Ca^{2+} -depleted ER due to persistent RyR2-mediated Ca^{2+} leak. Data are derived from biologically independent samples. All statistical tests were two sided.

Impaired long-term potentiation and hippocampal glucose metabolism in myocardial infarction mice

Field excitatory postsynaptic potentials (fEPSPs) were evaluated at the Schaffer collateral using a bipolar electrode placed at the CA3 and recording at the CA1 (Fig. 4a). Hippocampal slices obtained from MI mice showed decreased LTP as compared to slices obtained from SHAM animals ($P = 0.01$). S107 treatment reversed this effect ($P = 0.001$), with slices eliciting the same LTP response as SHAM, while treatment with ARM036 had no effect on hippocampal synaptic plasticity, resulting in impaired LTP in comparison to SHAM animals ($P = 0.01$). In addition, treatments with propranolol ($P = 0.01$) and SD-208 ($P = 0.005$) prevented MI-induced LTP deficits (Fig. 4b, c). Importantly, MI and treatment with the various compounds after MI had no effect on basal synaptic transmission determined by the input–output curves (I–O; $P = 0.5$; Fig. 4d).

Thereafter, we used [18F]fluorodeoxyglucose (FDG) with positron emission tomography (PET) to measure energy consumption in neurons, which reflects neuronal communication signals and the integrative local neuronal activity⁵². Deteriorating brain glucose metabolism measured by FDG-PET has been used as a clinical marker for Alzheimer’s disease

diagnosis⁵². Thus, we evaluated hippocampal FDG metabolism in our experimental groups (Fig. 4e,f). Interestingly, hippocampal FDG metabolism was significantly reduced by ~30% in the MI-treated (70 • +/- 3, $P < 0.05$) and MI + ARM036-treated (80 • +/- 8, $P < 0.05$) groups compared to SHAM (100 • +/- 3). The BBB-permeant drug S107, propranolol and SD-208 significantly improved the hippocampal FDG metabolism (114 • +/- 13, 145 • +/- 26 and 138 • +/- 22, respectively, $P < 0.05$; Fig. 4e,f). Importantly, the reduced FDG metabolism in the hippocampi of MI mice was not the result of changes in brain blood flow, which were not reduced in HF mice as measured by a dynamic microPET scan of MI and SHAM mice, nor were there any significant changes in the blood gases including pH, O₂ or CO₂ levels, at 2 months after MI (Fig. 4g-j). Both decreased LTP and FDG metabolism are likely due to impaired neurotransmission.

RyR2-p.Ser2808Ala mice are protected against cognitive dysfunction

To further evaluate the specific contribution of RyR2 to CD in HF, we used a mouse model with RyR2 phospho-mimetic PKA phosphorylation on Ser2808 causing RyR2 Ca²⁺ leak (RyR2-p.Ser2808Asp)^{26,31,53} and compared it to a non-leaky RyR2 mouse model that is protected against RyR2 Ca²⁺ leak due to the genetic ablation of the RyR2 PKA-phosphorylation site Ser2808 (RyR2-p.Ser2808Ala)^{26,31,54} (see cardiac function in Supplementary Table 5).

RyR2-p.Ser2808Ala-MI mice were protected against impaired locomotive activity and behavioral abnormalities and exhibited better learning and memory compared to RyR2-p.Ser2808Asp mice. S107 treatment improved the short-term memory and reduced the disinhibited behavior of the RyR2-p.Ser2808Asp mice (Extended Data Fig. 1). To ascertain the specific contribution of the RyR2 isoform in this process, we evaluated the CD of genetically altered mice harboring a leaky RyR1 isoform (RyR1-p.Ser2844Asp). We did not detect any cognitive impairment in these mice compared to controls (Extended Data Fig. 2). Moreover, RyR2-p.Ser2808Ala-MI were protected against RyR2 PTM and Ca²⁺ leak (Extended Data Fig. 3).

RyR2-mediated endoplasmic reticulum Ca²⁺ leak upon adrenergic activation in heart failure

To determine whether the activation of the adrenergic pathway indeed causes neuronal RyR2-mediated ER Ca²⁺ leak, we used caffeine (10 mM), a well characterized RyR agonist to assess RyR2 function specifically in hippocampal neurons without interference of other cell types such as glial cells or astrocytes. Indeed, caffeine application induced a small Ca²⁺ release in the hippocampal neurons treated with isoproterenol (an adrenergic agonist), which was prevented by either propranolol or S107. Moreover, hippocampal neurons expressing RyR2-p.Ser2808Asp exhibited a reduced RyR2 caffeine-induced Ca²⁺ release compared to controls. Interestingly, S107 treatment restored caffeine-induced RyR2 Ca²⁺ release in neurons expressing RyR2-p.Ser2808Asp mutant (Fig. 5). These findings are in accordance with the beneficial effects of S107 and propranolol on the long-term postsynaptic potentiation, brain glucose metabolism and the cognitive function.

Gene expression changes and neurodegenerative pathways in heart failure

We analyzed the proteome of whole-cell lysates isolated from hippocampi of MI ($n = 4$) and SHAM ($n = 4$) mice. We obtained 6,049 proteins with at least one unique peptide and a 1% false discovery rate (FDR). A volcano plot of all proteins is shown in Fig. 6a. Based on the criteria of adjusted P value < 0.05 , fold change ≥ 1.5 , and unique peptides ≥ 2 , we found 737 differentially expressed unique proteins (MI versus SHAM). Among these, 425 proteins were upregulated and 312 were downregulated. The heat map of 737 differentially expressed proteins is shown in Fig. 6b. The MI and SHAM groups were separately clustered, and the four replicates of each group showed good reproducibility. We then performed Gene Ontology (GO) enrichment analyses of these changed proteins. The top ten significant GO terms for biological processes, molecular functions and cellular components are shown in Fig. 6c–e. The biological process GO analysis shows that the differentially expressed proteins were enriched for the following terms: synaptic organization, ion and neurotransmitter transport, synapse activity and plasticity (Fig. 6c). The molecular functions of these dysregulated proteins are mainly related to ion channel activity, transporter activity, GTPase regulator activity, and calmodulin binding (Fig. 6d). Significantly dysregulated proteins were located mainly at the synaptic membrane (Fig. 6e). We also analyzed KEGG (Kyoto Encyclopedia of Genes and Genomes) pathways and found significant enrichment of Ca²⁺ signaling pathways (Fig. 6f). These findings are in accordance with the defective RyR2 Ca²⁺ handling and CD that we observed in MI mice.

Based on the proteome data in the setting of defective Ca²⁺ regulation, we selected four proteins for further study. These four proteins were from the most enriched synaptic transmission pathways that are regulated by Ca²⁺, located near the synaptic membranes, involved in learning and memory process, and involved in neurotransmission as potential downstream signals of leaky RyR2. These selections included synaptosomal-associated protein 25 (SNAP25), vesicle-associated membrane protein 8 (VAMP8), synaptogamin-2 (SYT2) and complexin3 (CPLX3). We analyzed their protein expression levels by immunoblot in individuals with HF, and in SHAM and MI mice with or without each of the aforementioned treatments. We found decreased VAMP8 and CPLX3 expression in hippocampi of individuals with HF and MI mice compared to SHAM mice, while SNAP25 and SYT2 expression were increased, confirming our proteomic analyses. These data indicate a potential role for the SNARE signaling pathway in HF⁵⁵. S107, propranolol and SD-208 treatment, but not ARM036, restored the expression of these proteins to the control levels ($P < 0.05$, $n = 4$ –9 per group; Fig. 7a–e).

Next, we performed GSEA with the canonical pathway and GO gene sets. The top 20 (activated and suppressed) significant GO terms for biological processes, molecular function and cellular components are shown in Extended Data Fig. 5. Interestingly, there was enrichment of GO terms related to mitochondria and neurotransmission as well as oxidative phosphorylation pathways (Extended Data Figs. 5 and 6a), which is potentially due to mitochondrial Ca²⁺ overload (see below), which would stimulate the activity of the tricarboxylic acid cycle and enhance the respiratory chain complex activity by providing more substrates. We also observed significant enrichment of neurodegenerative disease pathways, including those for Alzheimer's disease, Huntington's disease and Parkinson's disease (Extended Data Fig. 6b–d). These GO terms for oxidative phosphorylation defects, Parkinson's, Alzheimer's and Huntington's diseases detected by proteomics were also found at the RNA level (by RNA-sequencing analyses; Extended Data Figs. 7–9).

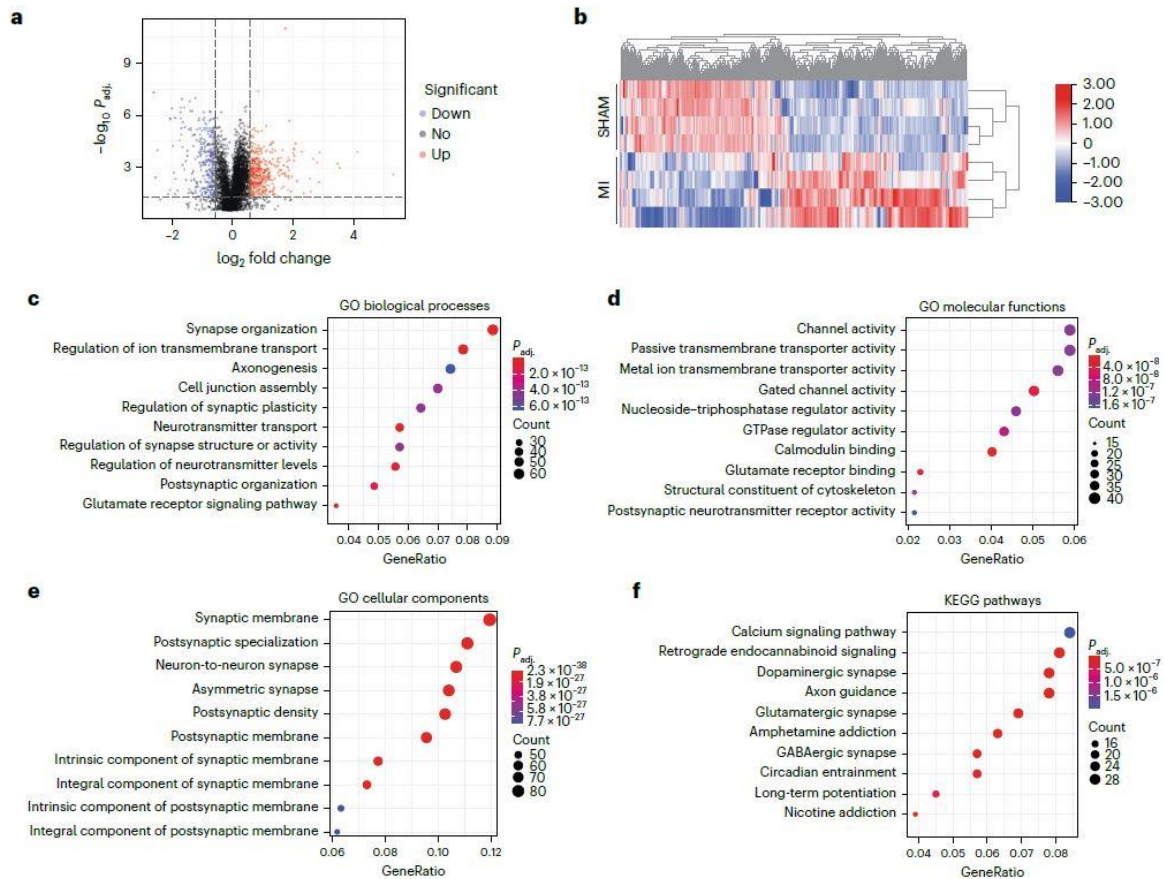


Fig. 6 | Quantitative proteomics analysis. **a**, Quantitative proteomics was performed on hippocampus samples from SHAM ($n = 4$) and MI ($n = 4$) mice. The Volcano plot shows differentially expressed proteins (P adjusted < 0.05 , fold change ≥ 1.5) in SHAM and MI mice. Red indicates upregulation, while blue represents downregulation of protein expression. Black indicates unchanged expression levels. **b**, The heat map of significantly dysregulated proteins (312 downregulated; 425 upregulated) The color scale bar shows the row normalized \log_2 protein abundance. **c-f**, Dot plots show top ten GO biological processes (**c**), molecular functions (**d**), cellular components (**e**) and KEGG pathways (**f**) that were enriched from differentially expressed proteins. Significantly changed protein abundance was determined by unpaired t -test with a threshold for significance of $P < 0.05$ (permutation-based FDR correction), fold change ≥ 1.5 , unique peptides ≥ 2 . Data are derived from biologically independent samples. All statistical tests were two sided. See Supplementary Table 7 for protein list.

Upstream signaling of leaky hippocampal RyR2

We also measured the hippocampal levels of norepinephrine and PKA activity. Hippocampal norepinephrine levels and PKA activity were increased in MI and RyR2-p.Ser2808Asp mice ($P < 0.05$, $n = 3$ in each group; Supplementary Table 5), in line with their respective reduced cardiac function (Supplementary Table 6). Interestingly, RyR2-p.Ser2808Ala-MI mice showed normal norepinephrine and PKA activity comparable to the RyR2-p.Ser2808Ala-SHAM mice. S107 and ARM036 treatments had no effect on brain norepinephrine nor PKA activity compared to untreated MI mice ($P = 0.9$, $n = 3$), because they act directly on RyR channels not on components of the adrenergic pathway.

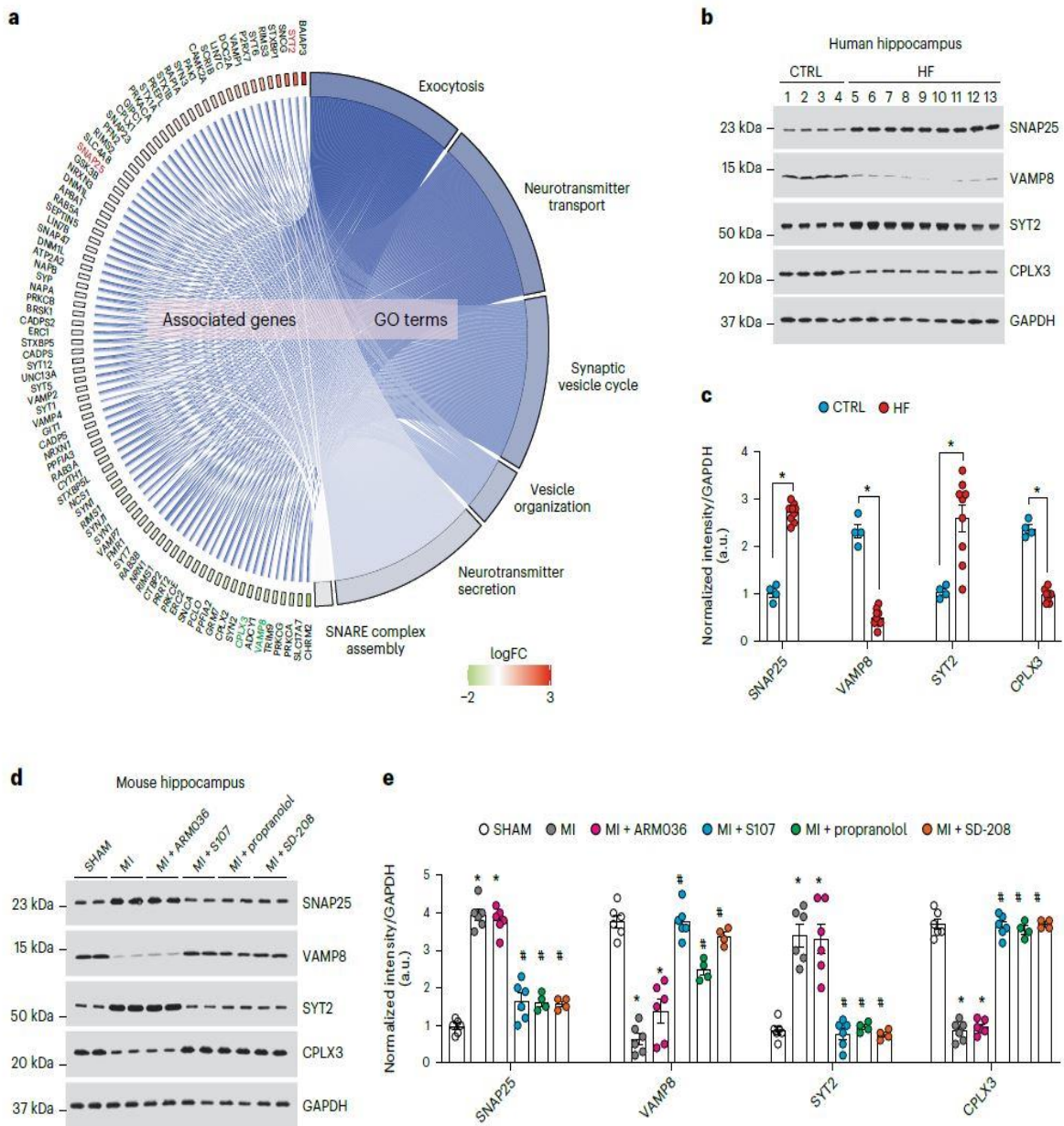


Fig. 7 | Altered synaptic protein expression in heart failure. **a**, Cohort plot representation of differentially expressed synaptic proteins (SHAM versus MI) from six significantly enriched synaptic transmission GO terms and generated by GOplot. The color map represents fold change of proteins (\log_2 scale). Selected proteins in the SNARE pathway are highlighted in red (upregulated) or green (downregulated). **b,c**, Immunoblots showing total expression of SNAP25, VAMP8, SYT2 and CPLX3, normalized to GAPDH in the hippocampi of controls ($n = 4$) and individuals with HF ($n = 9$). Individual values are shown with the mean \pm s.e.m. (t -test $*P < 0.05$, control versus individuals with HF). **d,e**, Immunoblots showing total expression of SNAP25, VAMP8, SYT2 and CPLX3, normalized to GAPDH in the hippocampi of SHAM ($n = 6$), MI ($n = 6$), MI + ARM036 ($n = 6$), MI + S107 ($n = 6$), MI + propranolol ($n = 4$) and MI + SD-208 ($n = 4$) mice. Individual values are shown with the mean \pm s.e.m. One-way ANOVA and Tukey's test post hoc correction for multiple comparisons, $*P < 0.05$, SHAM versus MI or MI + ARM036; $\#P < 0.05$ MI versus MI + S107, MI + propranolol or MI + SD-208. Data are derived from biologically independent samples. All statistical tests were two sided.

TGF- β has been implicated in CNS disorders including Alzheimer's disease^{56,57}. In accordance with our proteomic data, TGF- β levels and phosphorylated SMAD3 (a downstream signal of TGF- β) were increased in hippocampal tissues of individuals with HF and MI mice ($P < 0.05$). Furthermore, NADPH oxidase 2 (NOX2) binding to hippocampal

RyR2 was increased in both HF individuals and MI mice, which may account for the oxidation of RyR2 channels and ER Ca²⁺ leak in accordance with previous findings^{58–60} (Extended Data Fig. 4). TGF- β levels, phosphorylation of SMAD3 and NOX2 binding to hippocampal RyR2 were significantly reduced by propranolol and SD-208 treatment in line with the reduced RyR2 oxidation and phosphorylation levels shown in Fig. 3b,c. S107 only diminished the SMAD3 phosphorylation, whereas ARM036 had no effect on any of these changes (Extended Data Fig. 4).

Mitochondrial Ca²⁺ and oxidative overload in heart failure

We measured the mitochondrial Ca²⁺ content and reactive oxygen species (ROS) production and evaluated the expression and PTMs (phosphorylation) of Ca²⁺-activated enzymes that have been shown to be involved in neurodegenerative diseases such as Alzheimer's disease.

Our cohort plot of differentially expressed mitochondrial proteins shows an increase of the mitochondrial Rho GTPase 1 (RHOT1) in the MI mice (Extended Data Fig. 10a), which is a mitochondrial GTPase involved in mitochondrial fission during high Ca²⁺ conditions⁶¹. In line with the increased RyR2 Ca²⁺ leak, there was increased mitochondrial Ca²⁺ accumulation in MI mice ($P < 0.05$, $n = 12$). Interestingly, mitochondrial Ca²⁺ levels were significantly reduced by S107 treatment ($P < 0.05$, $n = 9$), indicating that leaky RyR2 channels are an upstream event of the mitochondrial Ca²⁺ overload (Extended Data Fig. 10b). Mitochondrial ROS production was significantly increased in the MI mice ($n = 9$) compared to the SHAM-operated group ($n = 12$, $P < 0.05$; Extended Data Fig. 10c). Although the mitochondrial ROS production was attenuated by S107, it did not reach statistical significance ($P = 0.2$), despite the reduction of the mitochondrial Ca²⁺ content. This is potentially due to irreversible damage that targets the electron transport chain that subsequently has led to increased electron transport chain protein expression levels observed in our proteomic analysis as a compensatory mechanism (Extended Data Figs. 5 and 6).

Alzheimer's disease-like signaling in heart failure

Abnormal Ca²⁺ regulation can contribute to the activation of Ca²⁺-dependent enzymes such as AMP-activated protein kinase (AMPK), cyclin-dependent kinase 5 (CDK5) and enhanced calpain activity^{26,62}. Activation of these enzymes in response to elevated cytosolic Ca²⁺ levels are upstream signals of both pTau and amyloid deposits in Alzheimer's disease brains^{26,63} and could be a major factor in the CD observed in HF. Hippocampal samples from both HF individuals and MI mice showed increased AMPK and GSK3 β phosphorylation (on Thr216) and CaMKII activity (Supplementary Table 6), compared to controls ($P < 0.05$). Interestingly, phosphorylation levels of Tau on Ser199/202/262 and Thr205 were significantly increased in both HF individuals and MI mice ($P < 0.05$). We also observed an increase in p25 expression, the neurotoxic activator of CDK5, which plays an important role in amyloid precursor protein processing in AD. Subsequently, the amyloid beta pathway may be activated, as BACE1 and β CTF levels were significantly increased in individuals with HF and MI mice (Supplementary Figs. 1 and 2). Finally, all of these changes were prevented/attenuated by treatment with S107, propranolol or SD-208 ($P < 0.05$, $n = 4$), but not by ARM036 (Supplementary Fig. 2).

Discussion

The major findings of this study are: (1) hippocampal neurons in HF have leaky RyR2, which correlates with behavioral abnormalities; (2) RyR2 channels are leaky due to stress-induced phosphorylation, oxidation, nitrosylation and depletion of the stabilizing subunit calstabin2; (3) hyper-adrenergic signaling and activation of TGF- β signaling are upstream signals of leaky RyR2; (4) excessive RyR2 Ca²⁺ leak is associated with mitochondrial dysfunction, impaired synaptic transmission and increased Tau pathway activation similar to that observed in Alzheimer's disease; (5) the Rycal drug (S107) prevents loss of the RyR2 stabilizing subunit calstabin2 and rescues the aforementioned subcellular events. Of note, we recently reported the binding site for the Rycal S107 (ref. 51) in RyR1 and ARM210 (ref. 50) in RyR2 using cryogenic electron microscopy, and have gained insights into its mechanism of action on leaky channels. Rycal drugs bind to a cleft in the RY1&2 domain of the channel where they stabilize interactions of key residues and reduce the flexibility between domains of the cytoplasmic shell, bringing the overall channel conformation from a primed state that is easily activated closer to the closed state thus preventing aberrant ER Ca²⁺ leak⁵⁰. In human and experimental models of HF, increased activity of the sympathetic nervous system⁶⁴ results in increased systemic catecholamine levels⁶⁵, that is, norepinephrine, an activator ligand of the adrenergic pathway. The improvement of the cognitive function and neuronal activity in the propranolol-treated MI mice, clearly shows that adrenergic signaling is an important component of cardiogenic dementia. Of note, this neurohormonal dysregulation that affects Ca²⁺ homeostasis is not limited to the heart and the brain of HF patients, but also impacts other organs, including skeletal muscle, and accounts for chronic fatigue, reduced exercise capacity and respiratory muscle weakness. Indeed, we have previously reported RyR1 remodeling in skeletal muscle of HF individuals, which impairs their exercise tolerance⁴².

We observed elevated brain norepinephrine levels and increased PKA activity associated with RyR2 Ca²⁺ leak in mice with failing hearts. This biochemical signature and dysfunction of RyR2 were correlated with behavioral abnormalities.

TGF- β , an upstream mediator of RyR2 oxidation via NOX2 enzymes^{58–60}, is also increased, thereby accounting for further oxidation of RyR channels and increased SR/ER Ca²⁺ leak in HF^{66,67}. In line with previously published studies⁶⁸, TGF- β inhibitor SD-208 significantly reduced RyR2 oxidation, rebound calstabin2 to the channel and decreased ER Ca²⁺ leak in the MI mice. Moreover, SD-208 improved LTP, brain glucose metabolism and the overall cognitive function of MI mice. Although the TGF- β family inhibitors have shown relative efficacy as an anticancer treatment, the SD-208 compound has rarely been tested for its effects on cognition. For instance, SD-208 was able to inhibit germinal matrix hemorrhage in a rat model of the disease with a partial recovery of the motor and cognitive function⁶⁹. SD-208 treatment improved the spatial learning in a rat model of HIV-1-associated neurocognitive disorders⁷⁰. Of note, this TGF- β inhibitor was used in our study to dissect the cellular mechanisms of cardiogenic dementia, but its potential as a drug candidate remains uncertain because of its cardiac toxicity and the side effects of blocking the physiological TGF- β signaling in healthy cells⁷¹. Our results indicate a beneficial effect of propranolol on cognition and memory in the context of cardiogenic dementia, in line with previously published studies showing improvement of cognitive function with beta-blocker therapy in different contexts such as hypertensive older individuals and patients Alzheimer's disease^{72,73}. Interestingly, propranolol displayed beneficial effects on cognition, especially

on sustaining cognitive performance over time in healthy individuals⁷⁴, and reduced amyloid and Tau pathology in Alzheimer's transgenic mice⁷⁵. Other studies have reported deleterious effects of beta blockers on cognitive function in patients after MI and in the general population^{76,77}. Because propranolol is extensively used to treat HF patients, a randomized clinical trial is necessary to resolve this controversy.

Mitochondrial Ca²⁺ accumulation, a downstream effect of TGF- β and leaky RyR2 channels was enhanced in MI mice, with significant upregulation of mitochondrial ROS production. These changes trigger a vicious cycle in which RyR2 leak leads to mitochondrial Ca²⁺ overload, which then produces ROS and further oxidizes RyR2 channels⁴⁶. Such a vicious cycle of Ca²⁺/ROS alteration could lead to gene and/or protein expression abnormalities that would worsen the prognosis of HF patients over time. The deep changes in the transcriptome and the proteome in the MI mice along with the epigenetic alterations we previously reported in the RyR2-p.Ser2808Asp mice serve as preliminary evidence of this hypothesis³¹.

Logically, oxidative stress and Ca²⁺ dysregulation would initiate a cellular response that would manifest at the level of neuronal gene expression. Support for this view stems from our observation of upregulation of 425 and downregulation of 312 proteins and genes in hippocampi from MI mice. Interestingly, the expression of key proteins regulated by Ca²⁺ and involved in synaptic transmission were modified including CPLX3, as well as SNAP25, SYT2 and VAMP8, which may explain, in part, the CD observed in our MI and RyR2-p.Ser2808Asp mice. For example, Ca²⁺ triggers rapid exocytosis of neurotransmitters from neurons. Such a process is mediated by synaptogamins, an abundant component of synaptic vesicles that binds Ca²⁺ ions through two C2 domains⁷⁸. Our data revealed a significant increase of the SYT2 isoform and SNAP25 at the protein expression level, which is an indicator of defective Ca²⁺-dependent exocytosis and altered hippocampal synaptic transmission in HF in line with the decreased LTP and brain glucose metabolism in the MI mice.

Furthermore, the changes in protein expression parallel some of the changes observed in models of neurodegenerative diseases. Postmortem studies of Alzheimer's disease brains have shown altered levels of several synaptic proteins, including SNAP25 and synaptogamins, components of the SNARE complex^{79,80}. Furthermore, cerebrospinal fluid (CSF) levels of SNAP25 (ref. ⁸¹) and synaptogamins⁸² have been assessed and found to be elevated in patients with Alzheimer's disease or middle cognitive impairment, compared to controls. To our knowledge, this is the first study reporting alterations in the hippocampal synaptic proteins and cognitive impairment in HF and providing a unique transcriptome and proteome library for the future mechanistic investigations and supported by in vivo and in vitro cognitive testing. This is particularly important for the initiation of large-scale clinical studies to assess some of these markers in the CSF or the plasma of HF patients as a predictive molecular fingerprint to monitor the onset and the progression of cognitive impairment in these patients. Finally, we report impaired hippocampal glucose metabolism in HF mice using [¹⁸F] FDG-PET scan imaging. This is a valuable neuroimaging tool for early detection of cardiogenic dementia and could be added as a clinical biomarker to support assessment and management of HF patients. Further studies to confirm its efficacy in early detection of CD are needed.

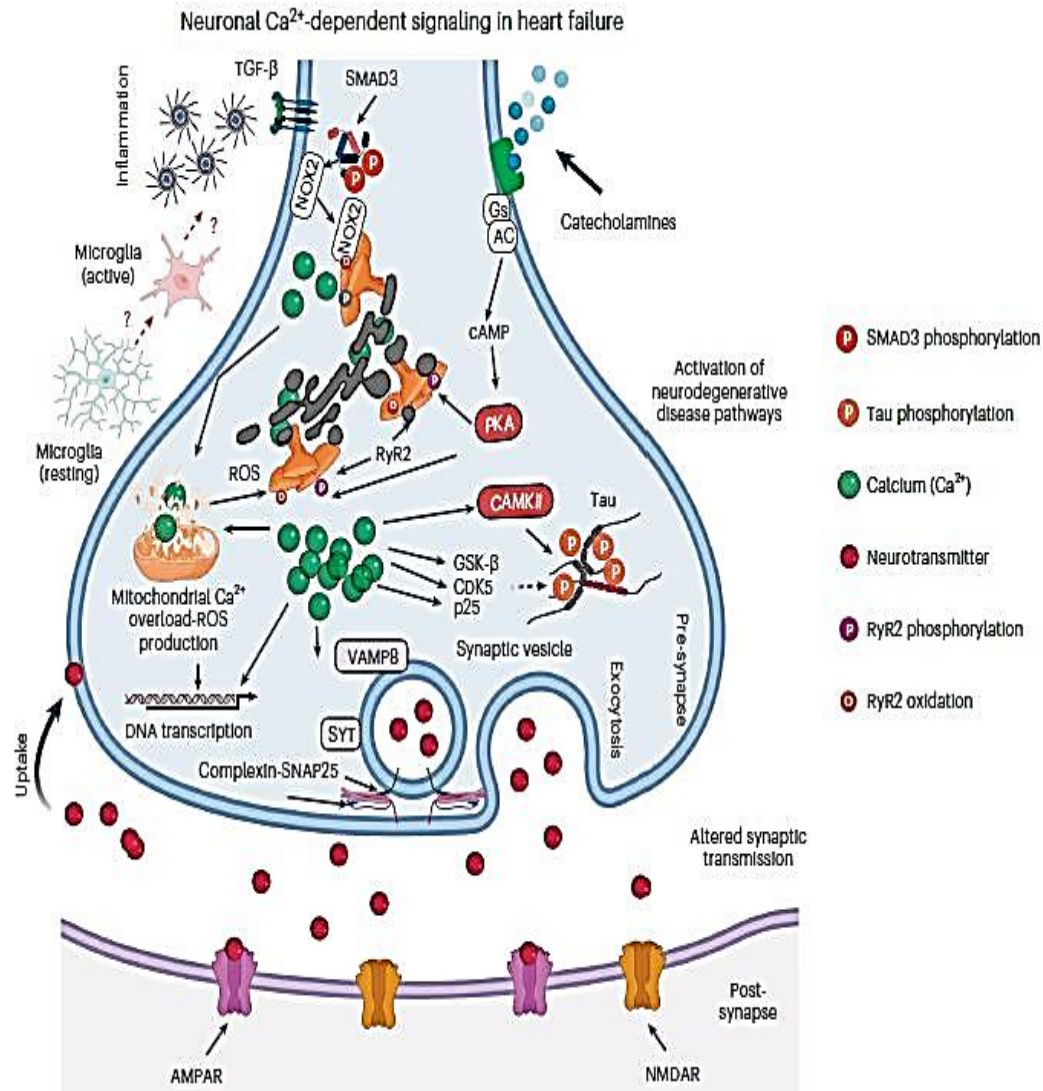


Fig. 8 | Neuronal Ca²⁺ signaling in heart failure. Increased catecholamine levels during HF activate PKA, which phosphorylates RyR2 on Ser2808 (Fig. 3). Increased inflammation in HF includes activation of the TGF- β pathway resulting in SMAD3 phosphorylation and upregulation of NOX2 and binding to RyR2 (Extended Data Fig. 4). NOX2 promotes oxidation of RyR2 channels^{58–60}. The combination of oxidation and phosphorylation of RyR2 results in ER Ca²⁺ leak (Fig. 3). Ca²⁺ leak through RyR2 leads to increased mitochondrial Ca²⁺ accumulation, which enhances mitochondrial ROS production (Extended Data Fig. 10). Therefore, a vicious cycle is created between the mitochondria and RyR2, where increased ER Ca²⁺ leak causes mitochondrial ROS production and increased mitochondrial ROS production further oxidizes RyR2 and renders it leakier. Chronic RyR2 Ca²⁺ leak depletes ER Ca²⁺ content and reduces the Ca²⁺ transient (Fig. 5) required for synaptic vesicle release during synaptic transmission (Figs. 4 and 7). Furthermore, oxidative stress and Ca²⁺ dyshomeostasis alter gene transcription (Extended Data Fig. 7), with a particular effect on proteins that are regulated by Ca²⁺ and involved in neurotransmission. Dysregulation of key proteins involved in synaptic transmission is reflected in the impaired LTP observed in the MI mice (Fig. 4b,c). Accumulation of Ca²⁺ in the cytosol activates Ca²⁺-dependent enzymes including CAMKII, GSK- β , CDK5 and p25, which subsequently leads to Tau phosphorylation, a hallmark of neurodegenerative disease (Supplementary Figs. 9 and 10). All these activated signaling cascades can be prevented, at least in part, by S107, a Rycal drug that reduces the ER Ca²⁺ leak. Gs, G protein; AC, adenylyl cyclase; cAMP, cyclic AMP; GSK- β , glycogen synthase kinase 3 beta. Created with BioRender.com.

Taken together, our data are in line with previous reports^{26,27,31,83} suggesting that defective Ca²⁺ plays an instrumental role in neurodegeneration and cognitive impairment. Further analyses of protein expression levels and PTMs showed significant upregulation of Ca²⁺-

dependent enzymes involved in Tau processing and Alzheimer's disease. These markers were found to be increased in a small cohort of individuals with coronavirus disease 2019 suspected of developing a forme fruste of Alzheimer's disease⁸³ due to defective Ca²⁺ regulation and inflammation. HF patients and MI mice exhibited increased TGF- β and SMAD3 phosphorylation levels that potentially play a role in cardiogenic dementia.

Increased adrenergic activity and inflammatory pathway activation in HF primarily impairs intracellular Ca²⁺ regulation. Excessive ER Ca²⁺ leak enhances oxidative stress, dysregulates neuronal gene/ protein expression and primes neurodegenerative pathways. These subcellular changes impair the learning and memory processes in HF, which is detrimental for patients' compliance to medication and early recognition of worsening symptoms. These pathways are summarized in Fig. 8.

Limitations of our study include a small sample size of only nine individuals with HF who had incomplete clinical information. We used multiple mouse models to overcome these limitations. Moreover, all individuals with HF were younger than controls, minimizing age-related confounding factors. Other factors such as individuals' backgrounds, socioeconomic status, hospitalization history and drug use could, however, contribute to CD.

References

1. Ambrosy, A. P. et al. The global health and economic burden of hospitalizations for heart failure: lessons learned from hospitalized heart failure registries. *J. Am. Coll. Cardiol.* 63, 1123–1133 (2014).
2. Ponikowski, P. et al. Heart failure: preventing disease and death worldwide. *ESC Heart Fail.* 1, 4–25 (2014).
3. Leto, L. & Feola, M. Cognitive impairment in heart failure patients. *J. Geriatr. Cardiol.* 11, 316–328 (2014).
4. McParland, C., Krishnan, B., Wang, Y. & Gallagher, C. G. Inspiratory muscle weakness and dyspnea in chronic heart failure. *Am. Rev. Respir. Dis.* 146, 467–472 (1992).
5. Huynh, K. Heart failure: HF-induced diaphragmatic atrophy and weakness. *Nat. Rev. Cardiol.* 14, 384 (2017).
6. Vogels, R. L. et al. Profile of cognitive impairment in chronic heart failure. *J. Am. Geriatr. Soc.* 55, 1764–1770 (2007).
7. Levin, S. N. et al. Cognitive status in patients hospitalized with acute decompensated heart failure. *Am. Heart J.* 168, 917–923 (2014).
8. Vogels, R. L., Scheltens, P., Schroeder-Tanka, J. M. & Weinstein, H. C. Cognitive impairment in heart failure: a systematic review of the literature. *Eur. J. Heart Fail.* 9, 440–449 (2007).
9. Dickson, V. V., Tkacs, N. & Riegel, B. Cognitive influences on self-care decision making in persons with heart failure. *Am. Heart J.* 154, 424–431 (2007).

10. Wu, J. R. et al. Factors influencing medication adherence in patients with heart failure. *Heart Lung* 37, 8–16 (2008).
11. Bouvy, M. L. et al. Effect of a pharmacist-led intervention on diuretic compliance in heart failure patients: a randomized controlled study. *J. Card. Fail.* 9, 404–411 (2003).
12. Evangelista, L. S., Berg, J. & Dracup, K. Relationship between psychosocial variables and compliance in patients with heart failure. *Heart Lung* 30, 294–301 (2001).
13. Murad, K. et al. Burden of comorbidities and functional and cognitive impairments in elderly patients at the initial diagnosis of heart failure and their impact on total mortality: the cardiovascular health study. *JACC Heart Fail.* 3, 542–550 (2015).
14. Hammond, C. A. et al. Long-term cognitive decline after newly diagnosed heart failure: longitudinal analysis in the CHS (Cardiovascular Health Study). *Circ. Heart Fail.* 11, e004476 (2018).
15. van den Hurk, K. et al. Heart failure and cognitive function in the general population: the Hoorn Study. *Eur. J. Heart Fail.* 13, 1362–1369 (2011).
16. Alosco, M. L. et al. Cerebral perfusion is associated with white matter hyperintensities in older adults with heart failure. *Congest. Heart Fail.* 19, E29–E34 (2013).
17. Jefferson, A. L. et al. Lower cardiac output is associated with greater white matter hyperintensities in older adults with cardiovascular disease. *J. Am. Geriatr. Soc.* 55, 1044–1048 (2007).
18. Hartupee, J. & Mann, D. L. Neurohormonal activation in heart failure with reduced ejection fraction. *Nat. Rev. Cardiol.* 14, 30–38 (2017).
19. Daniele, G., DiLucia, S., Masci, P. G. & Del Monte, F. Heart and brain: complex relationships for left ventricular dysfunction. *Curr. Cardiol. Rep.* 22, 72 (2020).
20. Sara, S. J. & Bouret, S. Orienting and reorienting: the locus coeruleus mediates cognition through arousal. *Neuron* 76, 130–141 (2012).
21. Reimer, J. et al. Pupil fluctuations track fast switching of cortical states during quiet wakefulness. *Neuron* 84, 355–362 (2014).
22. van den Brink, R. L. et al. Catecholaminergic neuromodulation shapes intrinsic MRI functional connectivity in the human brain. *J. Neurosci.* 36, 7865–7876 (2016).
23. Eschenko, O., Magri, C., Panzeri, S. & Sara, S. J. Noradrenergic neurons of the locus coeruleus are phase locked to cortical up-down states during sleep. *Cereb. Cortex* 22, 426–435 (2012).
24. McGinley, M. J., David, S. V. & McCormick, D. A. Cortical membrane potential signature of optimal states for sensory signal detection. *Neuron* 87, 179–192 (2015).

25. Francis, G. S. et al. Comparison of neuroendocrine activation in patients with left ventricular dysfunction with and without congestive heart failure. A substudy of the studies of left ventricular dysfunction (SOLVD). *Circulation* 82, 1724–1729 (1990).
26. Lacampagne, A. et al. Post-translational remodeling of ryanodine receptor induces calcium leak leading to Alzheimer's disease-like pathologies and cognitive deficits. *Acta Neuropathol.* 134, 749–767 (2017).
27. Dridi, H. et al. Role of defective calcium regulation in cardiorespiratory dysfunction in Huntington's disease. *JCI Insight* <https://doi.org/10.1172/jci.insight.140614> (2020).
28. Surmeier, D. J. et al. Calcium and Parkinson's disease. *Biochem. Biophys. Res. Commun.* 483, 1013–1019 (2017).
29. Augustine, G. J., Santamaria, F. & Tanaka, K. Local calcium signaling in neurons. *Neuron* 40, 331–346 (2003).
30. Hoffman, D. A., Sprengel, R. & Sakmann, B. Molecular dissection of hippocampal theta-burst pairing potentiation. *Proc. Natl Acad. Sci. USA* 99, 7740–7745 (2002).
31. Liu, X. et al. Role of leaky neuronal ryanodine receptors in stress-induced cognitive dysfunction. *Cell* 150, 1055–1067 (2012).
32. Santulli, G. & Marks, A. R. Essential roles of intracellular calcium release channels in muscle, brain, metabolism and aging. *Curr. Mol. Pharmacol.* 8, 206–222 (2015).
33. Mateos-Aparicio, P. & Rodriguez-Moreno, A. Calcium dynamics and synaptic plasticity. *Adv. Exp. Med. Biol.* 1131, 965–984 (2020).
34. Zalk, R. et al. Structure of a mammalian ryanodine receptor. *Nature* 517, 44–49 (2015).
35. Marx, S. O. et al. PKA phosphorylation dissociates FKBP12.6 from the calcium release channel (ryanodine receptor): defective regulation in failing hearts. *Cell* 101, 365–376 (2000).
36. Lehnart, S. E. et al. Phosphodiesterase 4D deficiency in the ryanodine-receptor complex promotes heart failure and arrhythmias. *Cell* 123, 25–35 (2005).
37. Meissner, G. & Henderson, J. S. Rapid calcium release from cardiac sarcoplasmic reticulum vesicles is dependent on Ca²⁺ and is modulated by Mg²⁺, adenine nucleotide, and calmodulin. *J. Biol. Chem.* 262, 3065–3073 (1987).
38. Kushnir, A., Shan, J., Betzenhauser, M. J., Reiken, S. & Marks, A. R. Role of CaMKII δ phosphorylation of the cardiac ryanodine receptor in the force frequency relationship and heart failure. *Proc. Natl Acad. Sci. USA* 107, 10274–10279 (2010).
39. Shan, J. et al. Phosphorylation of the ryanodine receptor mediates the cardiac fight or flight response in mice. *J. Clin. Invest.* 120, 4388–4398 (2010).

40. Reiken, S. et al. PKA phosphorylation activates the calcium release channel (ryanodine receptor) in skeletal muscle: defective regulation in heart failure. *J. Cell Biol.* 160, 919–928 (2003).
41. Marks, A. R. A guide for the perplexed: towards an understanding of the molecular basis of heart failure. *Circulation* 107, 1456–1459 (2003).
42. Rullman, E. et al. Modifications of skeletal muscle ryanodine receptor type 1 and exercise intolerance in heart failure. *J. Heart Lung Transplant.* 32, 925–929 (2013).
43. Lunde, P. K. et al. Effects of congestive heart failure on Ca²⁺ handling in skeletal muscle during fatigue. *Circ. Res.* 98, 1514–1519 (2006).
44. Santulli, G. et al. Calcium release channel RyR2 regulates insulin release and glucose homeostasis. *J. Clin. Invest.* 125, 4316 (2015).
45. Marx, S. O. et al. Phosphorylation-dependent regulation of ryanodine receptors: a novel role for leucine/isoleucine zippers. *J. Cell Biol.* 153, 699–708 (2001).
46. Santulli, G., Xie, W., Reiken, S. R. & Marks, A. R. Mitochondrial calcium overload is a key determinant in heart failure. *Proc. Natl Acad. Sci. USA* 112, 11389–11394 (2015).
47. Komada, M., Takao, K. & Miyakawa, T. Elevated plus maze for mice. *J. Vis. Exp.* <https://doi.org/10.3791/1088> (2008).
48. Bevins, R. A. & Besheer, J. Object recognition in rats and mice: a one-trial non-matching-to-sample learning task to study ‘recognition memory’. *Nat. Protoc.* 1, 1306–1311 (2006).
49. Morris, M. D. & Gebhart, G. F. Antianxiety agents and emotional behavior, an information processing analysis. *Prog. Neuropsychopharmacol.* 5, 219–240 (1981).
50. Miotto, M. C. et al. Structural analyses of human ryanodine receptor type 2 channels reveal the mechanisms for sudden cardiac death and treatment. *Sci. Adv.* 8, eabo1272 (2022).
51. Melville, Z. et al. A drug and ATP binding site in type 1 ryanodine receptor. *Structure* 30, 1025–1034 (2022).
52. Rocher, A. B., Chapon, F., Blaizot, X., Baron, J. C. & Chavoix, C. Resting-state brain glucose utilization as measured by PET is directly related to regional synaptophysin levels: a study in baboons. *Neuroimage* 20, 1894–1898 (2003).
53. Shan, J. et al. Role of chronic ryanodine receptor phosphorylation in heart failure and beta-adrenergic receptor blockade in mice. *J. Clin. Invest.* 120, 4375–4387 (2010).
54. Bussiere, R. et al. Amyloid beta production is regulated by beta2-adrenergic signaling-mediated post-translational modifications of the ryanodine receptor. *J. Biol. Chem.* 292, 10153–10168 (2017).
55. Rothman, J. E. The principle of membrane fusion in the cell (Nobel lecture). *Angew. Chem. Int. Ed. Engl.* 53, 12676–12694 (2014).

56. Webster, K. M. et al. Inflammation in epileptogenesis after traumatic brain injury. *J. Neuroinflammation* 14, 10 (2017).
57. Das, P. & Golde, T. Dysfunction of TGF-beta signaling in Alzheimer's disease. *J. Clin. Invest.* 116, 2855–2857 (2006).
58. Dridi, H. et al. Ryanodine receptor remodeling in cardiomyopathy and muscular dystrophy caused by lamin A/C gene mutation. *Hum. Mol. Genet.* 29, 3919–3934 (2021).
59. Souvannakitti, D. et al. NADPH oxidase-dependent regulation of T-type Ca²⁺ channels and ryanodine receptors mediate the augmented exocytosis of catecholamines from intermittent hypoxia-treated neonatal rat chromaffin cells. *J. Neurosci.* 30, 10763–10772 (2010).
60. Donoso, P. et al. Stimulation of NOX2 in isolated hearts reversibly sensitizes RyR2 channels to activation by cytoplasmic calcium. *J. Mol. Cell. Cardiol.* 68, 38–46 (2014).
61. Grossmann, D., Berenguer-Escuder, C., Chemla, A., Arena, G. & Kruger, R. The Emerging role of RHOT1/Miro1 in the pathogenesis of Parkinson's disease. *Front. Neurol.* 11, 587 (2020).
62. Saito, K., Elce, J. S., Hamos, J. E. & Nixon, R. A. Widespread activation of calcium-activated neutral proteinase (calpain) in the brain in Alzheimer disease: a potential molecular basis for neuronal degeneration. *Proc. Natl Acad. Sci. USA* 90, 2628–2632 (1993).
63. Reiken, S., Sittenfeld, L., Dridi, H., Liu, Y., Liu, X. & Marks, A. R. Alzheimer's-like signaling in brains of COVID-19 patients. *Alzheimers. Dement.* 18, 955–965 (2022).
64. Grassi, G., Quarti-Trevano, F. & Esler, M. D. Sympathetic activation in congestive heart failure: an updated overview. *Heart Fail. Rev.* <https://doi.org/10.1007/s10741-019-09901-2> (2019).
65. Rundqvist, B., Elam, M., Bergmann-Sverrisdottir, Y., Eisenhofer, G. & Friberg, P. Increased cardiac adrenergic drive precedes generalized sympathetic activation in human heart failure. *Circulation* 95, 169–175 (1997).
66. Suzuki, Y. J. & Ford, G. D. Redox regulation of signal transduction in cardiac and smooth muscle. *J. Mol. Cell. Cardiol.* 31, 345–353 (1999).
67. Zima, A. V. & Blatter, L. A. Redox regulation of cardiac calcium channels and transporters. *Cardiovasc. Res.* 71, 310–321 (2006).
68. Waning, D. L. et al. Excess TGF-beta mediates muscle weakness associated with bone metastases in mice. *Nat. Med.* 21, 1262–1271 (2015).
69. Manaenko, A., Lekic, T., Barnhart, M., Hartman, R. & Zhang, J. H. Inhibition of transforming growth factor-beta attenuates brain injury and neurological deficits in a rat model of germinal matrix hemorrhage. *Stroke* 45, 828–834 (2014).

70. Chompre, G., Martinez-Orengo, N., Cruz, M., Porter, J. T. & Noel, R. J. Jr. TGFbetaRI antagonist inhibits HIV-1 Nef-induced CC chemokine family ligand 2 (CCL2) in the brain and prevents spatial learning impairment. *J. Neuroinflammation* 16, 262 (2019).
71. de Streel, G. & Lucas, S. Targeting immunosuppression by TGF-beta1 for cancer immunotherapy. *Biochem. Pharmacol.* 192, 114697 (2021).
72. Gelber, R. P. et al. Antihypertensive medication use and risk of cognitive impairment: the Honolulu-Asia Aging Study. *Neurology* 81, 888–895 (2013).
73. Hajjar, I. et al. Cross-sectional and longitudinal association between antihypertensive medications and cognitive impairment in an elderly population. *J. Gerontol. A Biol. Sci. Med. Sci.* 60, 67–73 (2005).
74. Hahn, B., Olmstead, C. K., Yuille, M. B., Chiappelli, J. J. & Wells, A. K. Attention-enhancing effects of propranolol and synergistic effects with nicotine. *Cogn. Affect. Behav. Neurosci.* 20, 658–668 (2020).
75. Dobarro, M., Gerenu, G. & Ramirez, M. J. Propranolol reduces cognitive deficits, amyloid and tau pathology in Alzheimer's transgenic mice. *Int. J. Neuropsychopharmacol.* 16, 2245–2257 (2013).
76. Holm, H. et al. Beta-blocker therapy and risk of vascular dementia: a population-based prospective study. *Vascul. Pharmacol.* 125-126, 106649 (2020).
77. Steinman, M. A. et al. Association of beta-blockers with functional outcomes, death and rehospitalization in older nursing home residents after acute myocardial infarction. *JAMA Intern. Med.* 177, 254–262 (2017).
78. Huson, V. & Regehr, W. G. Diverse roles of synaptotagmin-7 in regulating vesicle fusion. *Curr. Opin. Neurobiol.* 63, 42–52 (2020).
79. Masliah, E. et al. Altered expression of synaptic proteins occurs early during progression of Alzheimer's disease. *Neurology* 56, 127–129 (2001).
80. Sze, C. I., Bi, H., Kleinschmidt-DeMasters, B. K., Filley, C. M. & Martin, L. J. Selective regional loss of exocytotic presynaptic vesicle proteins in Alzheimer's disease brains. *J. Neurol. Sci.* 175, 81–90 (2000).
81. Brinkmalm, A. et al. SNAP-25 is a promising novel cerebrospinal fluid biomarker for synapse degeneration in Alzheimer's disease. *Mol. Neurodegener.* 9, 53 (2014).
82. Ohrfelt, A. et al. The pre-synaptic vesicle protein synaptotagmin is a novel biomarker for Alzheimer's disease. *Alzheimers Res. Ther.* 8, 41 (2016).
83. Reiken, S. et al. Alzheimer's-like signaling in brains of COVID-19 patients. *Alzheimers Dement.* <https://doi.org/10.1002/alz.12558> (2022).